Eur. Phys. J. D **10**, 363–377 (2000)

THE EUROPEAN PHYSICAL JOURNAL D

EDP Sciences

Improved spectroscopic characterisation of the ground $X0^+(^1\Sigma^+)$, and lowest excited $A0^+(^3\Pi)$, $B1(^3\Sigma^+)$ and $D1(^1\Pi)$ energy states of CdNe complex in a wide range of internuclear separations

J. Koperski[1,a] and M. Czajkowski[2,b]

[1] Instytut Fizyki, Uniwersytet Jagielloński, ul. Reymonta 4, 30-059 Kraków, Poland
[2] Department of Physics, University of Windsor, Windsor, Ontario, N9B 3P4, Canada

Received 26 July 1999 and Received in final form 29 October 1999

Abstract. A first-time observed $A0^+_{v'=1} \rightarrow X0^+$ fluorescence as well as $D1_{v'=1} \rightarrow X0^+$ fluorescence, and $A0^+_{v'} \leftarrow X0^+_{v''=0,1,2}$, $B1_{v'} \leftarrow X0^+_{v''=0,1,2}$ and $D1_{v'} \leftarrow X0^+_{v''=0,1}$ excitation spectra of the CdNe van der Waals molecule have been recorded in the experiment of a continuous supersonic molecular beam crossed with a pulsed dye laser beam. A rigorous, improved analysis based on complete and simultaneous theoretical simulation of bound-free and bound-bound parts of the spectra is presented. Several controversies concerning interpretation of the $B1(^3\Sigma^+) \leftarrow X0^+(^1\Sigma^+)$ transition and determination of the CdNe ground state dissociation energy is explained and new approaches are postulated. The analysis indicates that a Morse function combined with an adequate term describing a long-range approximation represents the potential energy curve of the $A0^+(^3\Pi)$, $B1(^3\Sigma^+)$, $D1(^1\Pi)$ and $X0^+(^1\Sigma^+)$ states *below* the dissociation limit. In the simulation of the $A0^+(^3\Pi) \rightarrow X0^+(^1\Sigma^+)$ and $D1(^1\Pi) \rightarrow X0^+(^1\Sigma^+)$ bound-free spectra the Morse potential was found to be a good representation of the repulsive wall of the ground-state PE curve *above* the dissociation limit, over the internuclear separation range of $R = 3.15-3.75$ Å. All spectroscopic characteristics for the $B1$ and $X0^+$ as well as for the $A0^+$ and $D1$ states obtained in this work are compared with those of other experiments and theoretical calculations.

PACS. 33.20.Lg Ultraviolet spectra – 33.20.Vq Vibration-rotation analysis – 33.15.Fm Bond strengths, dissociation energies

1 Introduction

The recent advances in laser cooling and optical trapping techniques have been largely responsible for the renewed interest in the study of the region of the internuclear separations, which is responsible for the long-range forces between atoms in a molecule. Among the various techniques available diatomic molecular spectroscopy has proved to be the most effective and precise way to obtain information about the long-range interaction between two entities [1]. Furthermore, in the rapidly evolving field of matter-wave interferometry, in order to determine an index of refraction of a rare-gas medium for atomic waves it is necessary to know the interatomic potential of metal (Me)-rare gas (RG) systems not only in the long-range limit, but also in the short-range as well as in the bound well region [2]. Therefore, the knowledge about the interatomic potentials in the widest possible range of internuclear separations is highly desirable. Methods of extracting this information from experimental evidence are developing rapidly and they are implemented from all different branches of molecular spectroscopy, particularly from laser spectroscopy of van der Waals (vdW) complexes.

The weakly bound vdW molecules of IIb-group Me (Me = Zn, Cd, Hg) and RG (RG = He, Ne, Ar, Kr, Xe) atoms have been the subject of numerous recent studies [3–5]. In particular, investigators have been employing electronic transitions in CdRG vdW complexes formed in supersonic free jets to characterise their lowest excited as well as their ground electronic energy states. One of them, $D(\Omega = 1$ or $^1\Pi$-Hund's case c or a, respectively), correlates to the 5^1P_1, whereas two other, $A(\Omega = 0^+$ or $^3\Pi)$ and $B(\Omega = 1$ or $^3\Sigma^+)$, to the 5^3P_1, and the ground $X(\Omega = 0^+$ or $^1\Sigma^+)$ to the 5^1S_0 atomic cadmium asymptotes. In 1985, for the first time an excitation spectrum of the $A0^+ \leftarrow X0^+$ and $B1 \leftarrow X0^+$ transitions of CdNe molecule was reported by Kowalski *et al.* [6].

[a] e-mail: ufkopers@cyf-kr.edu.pl
[b] e-mail: mczajko@server.uwindsor.ca

Then, the high-resolution excitation spectra of the $A0^+ \leftarrow X0^+$ transition were presented by Kvaran *et al.* [7] and the spectroscopic characterisation of the $A0^+$ electronic energy state was proposed. A Morse potential along with a Lennard-Jones (12-6)-type correction at larger internuclear separations were chosen as representative for the $A0^+$-state potential energy (PE) curve. Soon afterwards, a spectroscopic characterisation of the CdNe ground $X0^+$ and lowest excited singlet $D1$ states was reported by Funk *et al.* [8]. They represented the upper state by a Morse and the ground state by a Buckingham-type potential based on their data from high-resolution excitation spectra of the $D1 \leftarrow X0^+$ transition and from fluorescence spectrum of the $D1_{v'=1} \rightarrow X0^+$ transition, respectively. A repeated, more complex analysis of the excitation spectra in $A0^+ \leftarrow X0^+$, $B1 \leftarrow X0^+$ and $D1 \leftarrow X0^+$ transitions of the CdNe was presented by Bobkowski *et al.* [9] and Czajkowski *et al.* [10]. All three excited states and the ground state were represented by Morse functions in the region of their potential wells, and a postulate of linear dependence of the dissociation energy of CdRG molecules on RG atom polarizability led to the development of an empirical calculation of dissociation energies and bond lengths for various states of vdW complexes [10] (note, that the singlet $D1(^1\Pi)$ molecular electronic state is called by Breckenridge and co-workers a $C^1\Pi_1$ state [8]).

Up to the present, despite the number of articles published [6–10], there are several controversies that still exist in the determination of the interatomic potentials for various electronic molecular states of the CdNe complex. First of all, the excitation spectrum of the $B1 \leftarrow X0^+$ transition, presented and analysed twice in references [6,9], seems to be incorrectly interpreted. Comparing to an analogous very well-known spectrum of the $B1 \leftarrow X0^+$ transition in HgNe molecule [11,12] the v'-progression in CdNe, which is detectable up to the dissociation limit of the $B1$ state, extends toward suspiciously high vibrational quantum numbers: $v' = 5$ [6], and $v' = 7$ [9]. The analogous $B1$ state in HgNe complex accommodates only three vibronic levels (up to $v'_{\max} = v'_{\mathrm{D}} - 1 = 2$) [11,12]. It is highly improbable that the $B1$-state potential well of CdNe would accommodate that large number of bound v' levels. Therefore, it is our opinion, that the erroneous interpretation was caused presumably by a considerably low signal-to-noise ratio in the previously reported spectra (see Fig. 2 in [6] and Fig. 1 in [9]). Secondly, in the first investigation [6] the dissociation energy of the CdNe ground state was determined *indirectly*, assuming knowledge on the dissociation energy of an excited state and the energy corresponding to a relevant $v' = 0 \leftarrow v'' = 0$ transition. The value $D''_{\mathrm{e}} = 39\ \mathrm{cm}^{-1}$ [6] was then adopted and used as a reference by others in their studies of CdRG complexes [7–9]. Recently, the bond depth of the CdNe ground state was examined by Czajkowski *et al.* [10]. In their studies they suggested a lower value for the D''_{e} (CdNe), however, no direct determination of the D''_0 (or D''_{e}), *e.g.* from so-called "hot" bands, was reported up to the present time. Consequently, the ground-state dissociation energy of CdNe established in the literature is somewhat uncertain and calls for a *direct* determination.

In this paper we present a first-time observed $A0^+_{v'=1} \rightarrow X0^+$ fluorescence spectrum as well as a repeated measurement of the $D1_{v'=1} \rightarrow X0^+$ fluorescence, and the excitation spectra of the $A0^+_{v'} \leftarrow X0^+_{v''=0,1,2}$, $B1_{v'} \leftarrow X0^+_{v''=0,1,2}$ and $D1_{v'} \leftarrow X0^+_{v''=0,1}$ transitions in the CdNe vdW molecule. Three aspects of our new investigation were particularly emphasised:

(1) an efficient detection of "hot" bands in the excitation spectra that would provide a direct information on the D''_0,
(2) a good signal-to-noise ratio in the excitation spectrum of the $B1 \leftarrow X0^+$ transition in order to determine accurately the number of bound v' levels in the $B1$-state potential well,
(3) a separate detection of two "channels" of fluorescence that start from selectively excited vibrational levels in *different* electronic energy states and terminate on the *same repulsive part* of the ground-state PE curve.

The spectra were subjected to an improved and rigorous analysis based on a complete simulation of bound-free and bound-bound parts. The analysis allowed us to determine accurately spectroscopic constants for all four electronic states involved in the investigation. Particularly, the spectroscopic characteristics were improved in the case of the $B1$ and $X0^+$ states. Moreover, in the simulation of the $A0^+ \leftarrow X0^+$ progression we allowed for an influence of the intense atomic line on the FC-intensity distribution. This procedure changed our view on the previously evaluated value for the difference of the equilibrium internuclear separation, ΔR, in the $A0^+$ and ground states. The rotational analysis of the $v' = 0 \leftarrow v'' = 0$ band in the $A0^+ \leftarrow X0^+$ transition corroborated our view thoroughly. We found that a Morse function combined with an adequate long-range approximation represents well the interatomic PE curve of the $A0^+$, $B1$, $D1$ and $X0^+$ states *below* the dissociation limit. The dissociation energy D''_0 of the ground state was determined directly from the "hot" bands observed in excitation spectra of the $A0^+ \leftarrow X0^+$, $B1 \leftarrow X0^+$ and $D1 \leftarrow X0^+$ transitions. The simulation of the fluorescence spectra confirmed this result. Moreover, the repulsive part of the ground state *above* the dissociation limit was accurately determined in the range of 3.15−3.75 Å, and found to be represented by a Morse potential. All characteristics determined in this work were compared with those of experimental [6–10] and theoretical [13] results available in the literature.

2 Experimental

The arrangement of the apparatus was described previously [4]. Laser-induced fluorescence (LIF) was observed in an evacuated expansion chamber into which the Cd atoms, seeded in neon, were injected through a nozzle ($d = 150\ \mu$m in diameter). Depending on the spectral

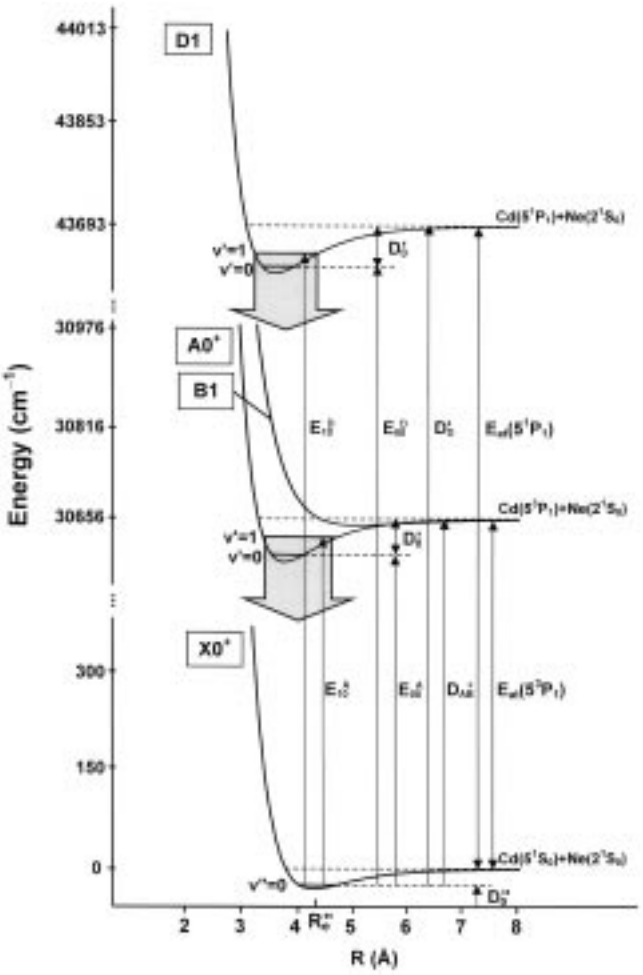

Fig. 1. Potential energy curves for the CdNe molecule in the $X0^+(^1\Sigma^+)$ ground and the $A0^+(^3\Pi)$, $B1(^3\Sigma^+)$ and $D1(^1\Pi)$ excited states. The curves are drawn according to the experimentally determined parameters using a Morse approximation. Absorption transitions, corresponding fluorescence bands, and E_{00} transitions as well as dissociation energies and dissociation limits are depicted.

region under study, the CdNe molecules in the beam were irradiated with the second harmonic output of a home-made dye laser utilising a 6.0×10^{-4} Ml^{-1} solution of DCM in dimethyl sulphoxide (for the $A0^+$, $B1 \leftarrow X0^+$ transitions in the vicinity of the triplet $5^3P_1-5^1S_0$ (3262 Å) Cd atomic transition) or with the second harmonic of the dye laser utilising a 7.0×10^{-4} Ml^{-1} solution of Coumarin 460 in methanol with a small admixture of Coumarin 480 in ethanol (for the $D1 \leftarrow X0^+$ transition in the vicinity of the singlet $5^1P_1-5^1S_0$ (2289 Å) Cd atomic transition). The dye laser was pumped with the second, or third harmonic output of a Nd:YAG laser, and a KDP-C, or a BBO-C frequency doubling crystal was simultaneously scanned with the dye laser over the range of $\lambda = 3255-3270$ Å, or $\lambda = 2285-2295$ Å, respectively. In case of the $A0^+$, $B1 \leftarrow X0^+$ transition the spectral line width of the dye laser output, monitored with a Fabry-Perot etalon, was found to be approximately 1/3 cm^{-1} and allowed us to observe rotationally resolved transitions in the $A0^+_{v'=0} \leftarrow X0^+_{v''=0}$ band. The $D1 \leftarrow X0^+$ transition was investigated with a somewhat spectrally wider laser output. The resulting spectra were monitored at right angle to the plane containing the crossed molecular and laser beams and focussed either, directly on the photocathode of the photomultiplier (PM) tube, or on the entrance slit of the HR−640 Jobin-Yvon monochromator, which was furnished with the PM tube mentioned above. The PM signal was recorded with a transient digitizer (Hewlett-Packard, HP54510A) and stored in a computer.

The beam source was operated at a temperature, T_0, of about 750–870 K (447–597 °C), which corresponds to the saturated Cd vapour pressure in the range of about 10–100 torr [14]. When recording the dispersed CdNe fluorescence spectra it was necessary to increase the reservoir temperature by 20–30 K, to compensate for the reduced radiation throughput of the monochromator. The carrier gas backing pressure, P_0, was maintained in the range from 8 atm to 11 atm while the X/d parameter was varied from 27 to 120, where X is the distance from the nozzle to the laser beam (excitation region). The efficiency of population cooling in v'' ground-state levels depends, among others, on the distance X from the orifice to the observation region [15,16]. Therefore, in order to detect "hot" bands in the excitation spectra it was necessary to choose small values of X.

Figure 1 shows a partial PE diagram for CdNe molecule, consistent with results of this study. However, for the sake of brevity, all interatomic potentials in a whole range of internuclear separations were represented by Morse functions. All relations between excited-state dissociation limit of the $A0^+$ (or $B1$) and $D1$ states, $D'_{\rm AB}$ and $D'_{\rm D}$, respectively, and between the dissociation energies, D'_0 and D''_0, as well as the energies corresponding to the atomic, $E_{\rm at}(5^3P_1)$, $E_{\rm at}(5^1P_1)$, and the $A0^+_{v'=0} \leftarrow X0^+_{v''=0}$, $B1_{v'=0} \leftarrow X0^+_{v''=0}$ and $D1_{v'=0} \leftarrow X0^+_{v''=0}$ transitions, are depicted. The value for the equilibrium internuclear separation in the ground state, $R''_{\rm e}$ was evaluated using a rotational analysis as well as a Liuti and Pirani method [17]. As will be seen from the analysis of the excitation spectra the equilibrium internuclear separations, $R'_{\rm e}(A0^+)$ and $R'_{\rm e}(D1)$ in the $A0^+$ and $D1$ state, respectively are smaller than $R''_{\rm e}$ [4–8]. Hence, in the fluorescence emitted from a selectively excited v' level in the $A0^+$ or $D1$ state both, bound-bound (discrete) and bound-free (continuous) bands, generally called Condon internal diffraction (CID) patterns [18], were detected. Here, a term "reflection spectra" should be used, as was appropriately pointed out by Tellinghuisen [19]. In the case of the $B1$ excited state the relation between $R'_{\rm e}(B1)$ and $R''_{\rm e}$ is different. There is no spatial overlap between the bound well of the excited state and the repulsive part of the ground state. Therefore, in the resulting $B1 \rightarrow X0^+$ fluorescence only bound-bound vibrational transitions are expected to be observed.

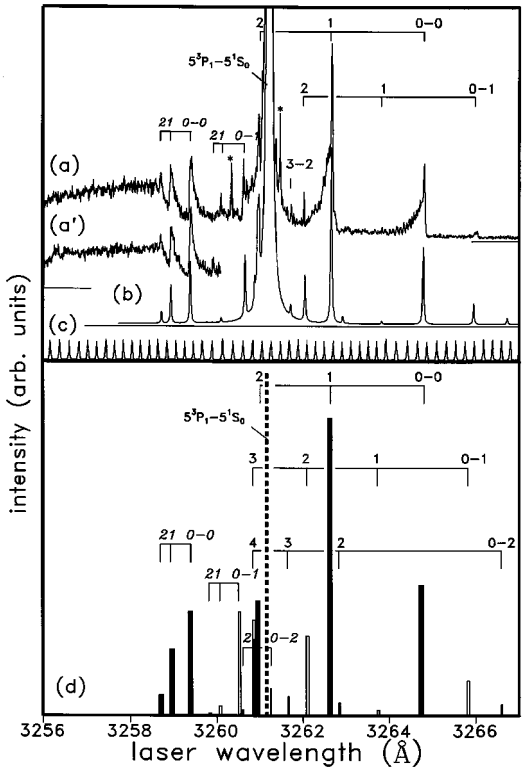

Fig. 2. (a) $A0^+(^3\Pi)$, $B1(^3\Sigma^+) \leftarrow X0^+(^1\Sigma^+)$ transitions in the excitation spectrum of the CdNe molecule recorded for $X/d = 60$ ($X = 9$ mm), $d = 150$ μm, $T_{\rm oven} = 850$ K, and $P_0 \approx 8.2$ atm; (a') as in (a) but for $X/d = 87$ ($X = 13$ mm) and $P_0 \approx 10.9$ atm; (*), unidentified bands; (b) theoretical simulation of the total $A0^+$, $B1 \leftarrow X0^+$ excitation spectrum, the FWHM of 0.3 cm^{-1} was used for the laser convolution function; (c) laser-fundamental frequency marking fringes recorded using 1 cm^{-1} FSR etalon.

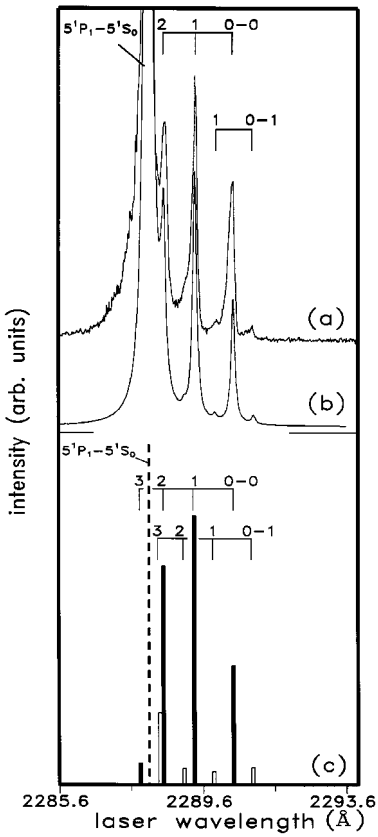

Fig. 3. (a) $D1(^1\Pi) \leftarrow X0^+(^1\Sigma^+)$ transition of the excitation spectrum of the CdNe molecule recorded for $X/d = 60$ ($X = 9$ mm), $d = 150$ μm, $T_{\rm oven} = 775$ K, and $P_0 = 10.9$ atm; (b) theoretical simulation of the total $D1 \leftarrow X0^+$ excitation spectrum, the FWHM of 2.3 cm^{-1} was used for the laser convolution function.

3 Results and improved spectroscopic characterisation of the $A0^+(^3\Pi)$, $B1(^3\Sigma^+)$, $D1(^1\Pi)$ and $X0^+(^1\Sigma^+)$ energy states

3.1 Excitation spectra of the $A0^+ \leftarrow X0^+$, $B1 \leftarrow X0^+$ and $D1 \leftarrow X0^+$ bound-bound transitions

Figures 2a, 2a' and 3a show the $A0^+$, $B1 \leftarrow X0^+$ and $D1 \leftarrow X0^+$ transitions in the excitation spectrum, which were observed on the short and long-wavelength sides of the Cd 3262 Å and on the long-wavelength side of the Cd 2289 Å lines, respectively. Two v'-progressions resulting from the $B1_{v'} \leftarrow X0^+_{v''=0}$ and $A0^+_{v'} \leftarrow X0^+_{v''=0}$ transitions as well as v'-progression, which results from the $D1_{v'} \leftarrow X0^+_{v''=0}$ transition are shown in Figures 2 and 3, respectively. Also in Figures 2 and 3 we can recognise some well defined "hot" bands that originate from $v'' = 1$, 2 and $v'' = 1$ of the ground-state vibronic levels, respectively, which were efficiently populated in the process of expansion. The "hot" bands were not observed (or if observed then their frequencies were not well defined) in earlier investigations [6–10]. In contrary to that, in this experiment the production of "hot" bands was carefully controlled, and the recorded spectra were analysed by means of a simulation assuming the "best fit" of the vibrational temperature $T_{\rm V}$ in the expansion beam. Both v'-progressions in the $A0^+_{v'} \leftarrow X0^+_{v''=0}$ and $D1_{v'} \leftarrow X0^+_{v''=0}$ transitions are similar to those of references [6,7,9] and references [8,10]. However, the spectra presented in this work were detected with a significantly better signal-to-noise ratio. The v'-assignment in the $A0^+ \leftarrow X0^+$ and $D1 \leftarrow X0^+$ spectra has been confirmed in all cases by means of observation of the $A0^+ \rightarrow X0^+$ and $D1 \rightarrow X0^+$ fluorescence spectra. They agree well with those of references [6–10]. Special attention has to be paid to a large number of "hot" bands which is present in the $B1 \leftarrow X0^+$ spectrum as well as to the $B1_{v'} \leftarrow X0^+_{v''=0}$ progression itself.

One of the main goals of this work was to repeat the measurements of $B1 \leftarrow X0^+$ transition reported in references [6,9] in order to verify their characterisation. The results of the measurements presented here do not agree with those reported previously for the CdNe complex [6,9] but, their seem to be consistent with the observations performed for the analogous transition in the HgNe molecule [11,12]. The difference between the equilibrium internuclear separations in the $B1$ and $X0^+$ states

ensures that the spectrum consists of both, the three $v' = 0 \leftarrow v'' = 0$, $1 \leftarrow 0$ and $2 \leftarrow 0$ bands and the distinct dissociation continuum (see Figs. 2a and 2a'), which means that there are only three bound vibronic levels accommodated by the $B1$-state potential well. The signal-to-noise ratio excludes any misinterpretation, *i.e.* the v'-progression is very pronounced and repeatable under different conditions of the expansion. We simulated the Franck-Condon (FC) factors corresponding to the "cold" $v' \leftarrow v'' = 0$ and "hot" $v' \leftarrow v'' = 1, 2$ progressions in the $A0^+$, $B1 \leftarrow X0^+$ transition as well as the "cold" $v' \leftarrow v'' = 0$ and "hot" $v' \leftarrow v'' = 1$ progressions in the $D1 \leftarrow X0^+$ transition, respectively (see Figs. 2d and 3c). Having determined the amplitudes for all the FC factors we simulated then the *total spectra* of the $A0^+$, $B1 \leftarrow X0^+$ and $D1 \leftarrow X0^+$ transitions. They are shown in Figures 2b and 3b. The experimental traces from Figures 2a, 2a' and 3a were quite well reproduced assuming that the laser radiation is represented by a convolution function and has a width of 0.3 cm^{-1} and 2.3 cm^{-1} (FWHM), respectively. The conclusion agrees very well with our experimental determination of the laser bandwidth.

Furthermore, the T_V assumed in the simulation was in the range of 15–20 K. It is necessary to mention here that in the simulation of the total spectra we did not attempt to reproduce the dissociation continuum of the $B1$ state and "shading" of the vibrational bands. The main reason for the simulation was to show an influence of both, "hot" bands on the "cold" progression, and the neighbouring atomic line, which is large in amplitude, on the intensity distribution among particular vibrational bands. Ground and excited-states spectroscopic constants (ω_0, $\omega_0 x_0$) used in the simulation of the spectra from Figures 2a, 2a' and 3a were determined in the Birge-Sponer (BS) analysis (see below) and a Morse function was assumed as representative for the four states in the regions of internuclear separation which correspond to the observed $v' \leftarrow v''$ transitions. The FC patterns for the $A0^+ \leftarrow X0^+$, $B1 \leftarrow X0^+$ and $D1 \leftarrow X0^+$ transitions were simulated by a trial-and-error method. As a result, the differences $\Delta R_e = R'_e - R''_e$ between equilibrium internuclear separations in the respective excited and ground states were determined and they differ, especially for the $A0^+$ state, from those of references [8–10]. It is necessary to comment on a source of this difference. It is very likely that the simulations of the $A0^+ \leftarrow X0^+$ transition, which were made in references [7,9], did not allow for the influence of the very intense atomic line, especially on the intensity of the $A0^+_{v'=2} \leftarrow X0^+_{v''=0}$ band. In the spectrum (see Fig. 2) the band is almost overlapped with the atomic line. In reality (when isolated) its amplitude is smaller than observed. This substantially lowers the difference $\Delta R_e(A0^+)$.

3.2 Birge-Sponer and LeRoy-Bernstein analyses

There are two commonly used methods for the extrapolation of vibrational levels in order to determine dissociation energies. In the BS analysis [20], the decrease in vibrational spacing $\Delta G_{v+1/2}$ [21], as the dissociation limit is approached, is assumed to be linear, while in the LeRoy-Bernstein (LRB) analysis [22] the trend is described by a power law, with an appropriate exponent to describe the exact long-range interactions present. It should be noticed that a similar approach was independently developed by Stwalley [23]. Here, *both methods* are applied to determine molecular constants (mainly long-range coefficients) of the $A0^+$, $B1$, $D1$ and $X0^+$ states of the CdNe molecule. Their applicability depends on the range of internuclear separations within which the vibrational transitions were observed. However, a recently developed GvNDE-program of LeRoy [24,25] for fitting vibrational energies to the near-dissociation expansion (NDE) allows to determine the long-range potential characteristics even when the close-to-dissociation limit vibrational transitions are not measured. The program was successfully applied [25–27] and proved itself to be a good tool that *supplements* the BS and the "traditional" LRB procedures.

3.3 Excited states correlating to the 5^3P_1 and 5^1P_1 atomic asymptotes

3.3.1 B1($^3\Sigma^+$) state

Table 1 collects frequencies of vibronic bands observed in the $A0^+$, $B1 \leftarrow X0^+$ transitions as well as vibrational spacings $\Delta G_{v'+1/2}$ necessary in both, BS and LRB analyses. Moreover, the experimental frequencies are compared with those that were calculated during the simulation of the excitation spectra in Figures 2 and 3. Figure 4 presents BS plots for all four states analysed in this work. For the v'-progression of the $B1 \leftarrow X0^+$ transition the BS plot is *linear* (see Fig. 4a). The short extrapolation provides ω'_0, slope $\omega'_0 x'_0$, and hence $D'_0 = (\omega'_0)^2/4\omega'_0 x'_0$ (as well as ω'_e, $\omega'_e x'_e$ and D'_e [21]). Moreover, a long extrapolation, *i.e.* the intercept with the v' axis gives $v'_D = \omega'_0/2\omega'_0 x'_0$. Here $v'_D = 2.5$, which means that the $B1$-state potential well supports three bound vibrational levels. A relationship (see Fig. 1):

$$D'_B = E_{00}(B) + D'_0(B), \tag{1}$$

allows to determine a dissociation limit (with respect to $v'' = 0$) for the $B1$-state potential. The value obtained is 30 680.2 cm^{-1}. From the other hand, however, a long-range behaviour of the potential can be approximated by an expression $U'_B(R) = D'_B - \sum C_n R^{-n}$, where C_n is a constant, and n is determined by the nature of the long-range attractive interaction between the dissociating atoms. In the case of an analogous $B1 \leftarrow X0^+$ spectrum of HgAr molecule it had been shown [28] that the interaction is an induced dipole-induced dipole like in nature, and $n = 6$ is the *leading term* in the expression for the $U'_B(R)$. Therefore, it is justified to approximate the long-range part of the $B1$-state potential by the $C_6 R^{-6}$ term and to employ a "traditional" LRB method [22]. The vibrational first differences $\Delta G_{v'} = 1/2(E_{v'-1} - E_{v'+1})$ are related by the

Table 1. Centers of rotationally unresolved vibrational bands observed in the $A0^+(^3\Pi) \leftarrow X0^+(^1\Sigma^+)$ and $B1(^3\Sigma^+) \leftarrow X0^+(^1\Sigma^+)$ transitions of the CdNe molecule.

v′←v″	A0⁺←X0⁺ ν [cm⁻¹] expt.	A0⁺←X0⁺ ν [cm⁻¹] calcul. (BS) [a]	$\Delta G_{v'+1/2}$ expt.	Remarks	v′←v″	B1←X0⁺ ν [cm⁻¹] expt.	B1←X0⁺ ν [cm⁻¹] calcul. (BS) [a]	$\Delta G_{v'+1/2}$ expt.	Remarks
0←0	30621.7	30621.6	20.4		0←0	30673.3	30673.3	4.40	
1←0	30642.1	30642.0	16.3		1←0	30677.67	30677.6	2.24	
2←0	30658.4	30658.0	11.1		2←0	30679.9	30679.7		
3←0	30669.5	30669.5	7.5 [b]		0←1	30661.7	30662.0	4.4	
4←0	-	30676.8			1←1	30666.1	30666.4	2.2	
0←1	30610.2	30610.4	20.8		2←1	30668.3	30668.4		
1←1	30631.0	30630.8	15.5		0←2	30654.4	30654.6		
2←1	30646.6	30646.8	11.8		1←2	-	30659		within resonance line
3←1	30658.4	30658.4	7.2 [b]	overlapped with 2←0 transition	2←2	30660.9	30661		
4←1	30665.6	30665.6			1←3	-	30655.5		within resonance line
3←2	30651.1	30651							
4←2	30658	30658.2		overlapped with 2←0 and 3←1 transitions					
4←3	30654.4	30654.6	2.8 [b]						
5←3	30657.4	30657.3							

[a] Calculated frequencies with an assumption of anharmonic potential approximation.
[b] Calculated with a partial help of simulation procedure.

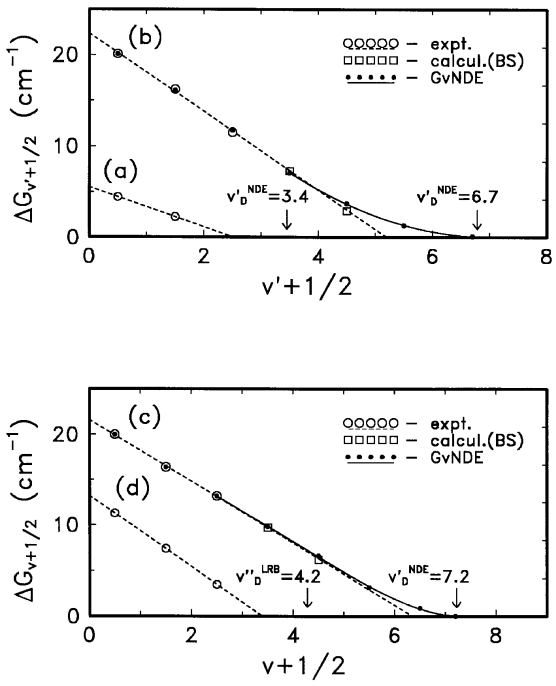

Fig. 4. Birge-Sponer plots for the v-progressions in the (a) $B1(^3\Sigma^+)$, (b) $A0^+(^3\Pi)$, (c) $D1(^1\Pi)$, and (d) $X0^+(^1\Sigma^+)$ energy states of CdNe; (○), experimental (for (a) and (b) see averaged values $\Delta G_{v'+1/2}$ from Tab. 2), and (□), calculated (within an anharmonic potential approximation) points are indicated. The short extrapolation and slope give ω_0 and $\omega_0 x_0$, respectively, while the long extrapolation provides v_D (those obtained from the "traditional" LRB, v_D^{LRB}, method and the GvNDE program, v_D^{NDE}, are marked as well). The long-range behaviour of the $\Delta G_{v+1/2}$, generated in the GvNDE program of LeRoy (•), is presented for comparison.

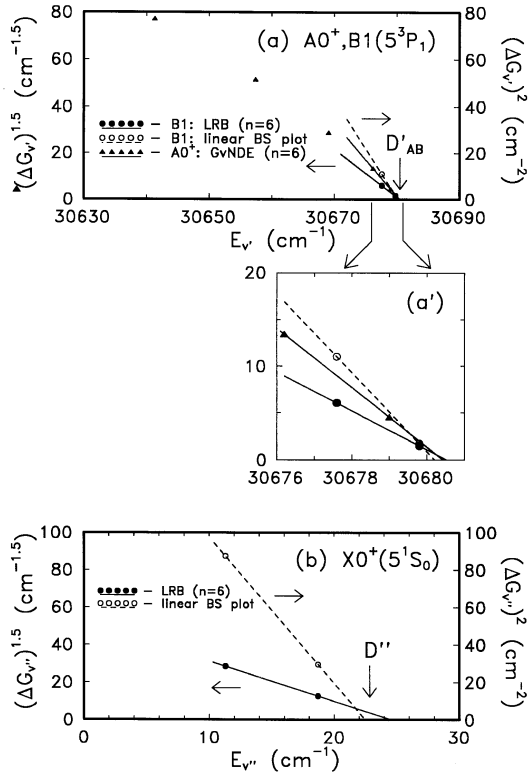

Fig. 5. LeRoy-Bernstein plot (according to Eq. (3)), for $n = 6$, constructed for the (a) $A0^+(^3\Pi)$ and $B1(^3\Sigma^+)$, and (b) $X0^+(^1\Sigma^+)$ energy states of CdNe molecule. A linear long extrapolation of the plot gives the dissociation limits: (a) $D'_{\rm AB}$, and (b) D''. Results of the "traditional" LRB method and GvNDE program are compared with that corresponding to the linear BS procedure [29]. Insert in (a') shows details of (a) close to the dissociation.

equation:

$$\Delta G_{v'}^{2n/(n+2)} = K_n^{2n/(n+2)}(D_{\rm B'} - E_{v'}), \qquad (2)$$

and the constant K_n is given by

$$K_n = [\hbar n \Gamma(1+1/n)]/[\mu^{1/2} C_n^{1/n} \Gamma(1/2+1/n)],$$

where $\hbar = h/2\pi$, μ, and Γ are Planck constant, reduced mass of the CdNe molecule, and gamma function, respectively. Figure 5a presents the LRB plot for the $B1$ state (assumed $n = 6$). The plot (full circles) is compared with that which corresponds to a linear BS characteristic (*i.e.* $\Delta G_{v'}^2$ *vs.* $E_{v'}$ [29,30]) of the $B1$ state up to the $D'_{\rm B}$ (empty circles). The dissociation limit determined assuming a vdW interaction is only 0.3 cm^{-1} larger than that from the BS plot (see Eq. (1)). Except the $D'_{\rm B}$, the LRB method provides the $C_6(B1)$ constant from equation (2) and the effective (in general non-integer) vibrational index at the dissociation limit, $v'_{\rm D}$ [22]. Figure 6 (full circles) shows a plot of $(D'_{\rm B} - E_{v'})^{(n-2)/2n}$ *vs.* v' for $n = 6$, according to the formula:

$$(D'_{\rm B} - E_{v'})^{(n-2)/2n} = (v'_{\rm D} - v')H_n, \qquad (3)$$

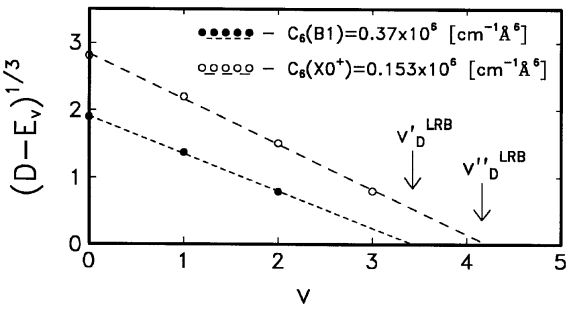

Fig. 6. Determination of the constant $H_{n=6}$ (slope) and the effective vibrational index $v_{\rm D}$ at the dissociation according to equation (5) applied for the $B1$ (full circles) and $X0^+$ (open circles) energy states of CdNe. An extrapolation through measured v provides: $H_6(B1) = 0.57$ cm$^{-1/3}$ hence $C_6(B1) = 0.37 \times 10^6$ cm^{-1}Å^6 (Eq. (4)), and $H_6(X0^+) = 0.66$ cm$^{-1/3}$ hence $C_6(X0^+) = 0.153 \times 10^6$ cm^{-1}Å^6. $v'_{\rm D}$ and $v''_{\rm D}$ are depicted.

where $H_n = [(n-2)/2n]K_n$. The plot gives $H_{n=6}$ and $v'_{\rm D}$ as the slope of a linear extrapolation and the intercept with the horizontal axis, respectively. The value of $v'_{\rm D}$(LRB) = 3.4 is very close to that from the BS procedure corroborating the result obtained for $D'_{\rm B}$. The leading coefficient $C_6(B1)$ was determined to be 0.37×10^6 cm^{-1}Å^6 and, therefore, the long-range potential is expressed by the formula $U'_{\rm B}(R) = 30\,680.5 - 0.37 \times 10^6 R^{-6}$ cm^{-1}Å^6. The $C_6(B1)$ obtained here should be compared with theoretical value of Brym who used Unsöld formula with an aid of Hartree-Fock approximation: $C_6(5^3{\rm P}_1) = 0.256 \times 10^6$ cm^{-1}Å^6 [31].

3.3.2 $A0^+(^3\Pi)$ state

Similarly, we used the BS plot to determine the Morse characteristics of the $A0^+$ state (see Fig. 4b, and Tab. 2). Because there is not sufficient experimental evidence close to the dissociation, to characterise the $A0^+$-state potential in the long-range limit, it is necessary to employ the GvNDE program of LeRoy [24,25]. In reference [24] the author provides a detailed description of the method and we shall not repeat here all the details. In the present case the *dominant* inverse-power term in the long-range $A0^+$ potential corresponds to $n = 6$ as well (*e.g.* [4,28,32–34]). With the $C_6(B1)$ determined above, $v'_{\rm D}$ from the BS analysis, and measured $E_{v'=0-2}$ as input parameters, and $D'_{\rm A} = 30\,680.5$ cm^{-1} which was kept fixed during the procedure the program generated $C_6(A0^+) = 0.367 \times 10^6$ cm^{-1}Å^6, $v'_{\rm D} = 6.7$ as well as the D'_0 and $D'_{\rm e}$ and remaining $E_{v'}$ values up to the dissociation limit (see Fig. 4b). A LRB plot constructed for the $A0^+$ state, according to data obtained using the GvNDE program, is compared with the LRB plot of $B1$ state and shown in Figure 5a. The linear regression was performed only for the levels closest to the dissociation limit, as advised by the author of the method [24]. It illustrates (see insert) that the $A0^+$ and $B1$ states have the

Table 2. Potential parameters of the CdNe molecule in the $X0^+(^1\Sigma^+)$, $A0^+(^3\Pi)$, $B1(^3\Sigma^+)$ and $D1(^1\Pi)$ energy states.

Designation	$X0^+(^1\Sigma^+)$		$A0^+(^3\Pi)$		$B1\ (^3\Sigma^+)$		$D1\ (^1\Pi)$	
	This work	Previous studies	This work	Previous studies	This work	Previous studies	This work	Previous studies
ω_0	13.2[a]	13[h]	22.8[a]	19.5[h]	5.5[a]	5.2[h]; 4.5[m]	21.8[a]	22.5[n]
$\omega_0 x_0$	1.94[a]	1.3[h]	2.2[a]	1.6[h]	1.1[a]	0.4[h]; 0.3[m]	1.78[a]	2.0[n]
D_0	22.4[a]	33[h]	59.0[a] 59.3[d]	66[h]	6.9[a]	18[h]; 17[m]	66.7[a] 66.9[d]	63.3[n]
ω_e	15.0[a]	13.2[i] 15.2[s]	24.9[a]	22.6[k] 25.8[s]	6.5[a]	4.8[m] 8.8[s]	23.5[a]	23.4[i] 24.5[n] 23.7[s]
$\omega_e x_e$	1.94[a]	1.15[i]	2.2[a]	1.6[k]	1.1[a]	0.3[m]	1.78[a]	1.8[i]; 2.0[n]
D_e	28.3[a]	39[h]; 55[s]	70.5[a] 70.8[d]	77[k]; 88[l] 115[s]	9.6[a]	21[h]; 19.3[m] 28[s]	77.6[a] 78.7[d]	58.9[i] 76[l]; 111[s]
$\Delta R_e = R_e' - R_e''$ (Å)	-	-	−0.56 ±0.02[b]; −0.53 ±0.01[g]	−1.0[m] −0.64[k] −0.9[s]	0.8±0.02[g]	0.7[m]	−0.68 ±0.02[g]	−0.65[l] −0.7[n]
R_e (Å)	4.32 ±0.02[b,g]; 4.31[f]	4.26[k] 4.13[s]	3.76 ±0.02[b,g]	3.62[k] 3.44[s]	5.12	4.98[m] 5.08[s]	3.60	3.61[i] 3.58[n];3.49[s]
D (with respect to $v''=0$)	22.4[a] 23.4[c]	-	30680.5[c]	-	30680.2[a] 30680.5[c]	-	43715.2[a]	-
α_{Cd} (a.u.)	41.0[e]	49.7[p] 40.3[r]	198[e]	-	198[e]	-	164.7[e]	-
C_6 (a.u.)	31.7[c]	128.8[i] 32.5[o]	76.1[d]	82.8[k] 53.1[o]	76.8[c]	53.1[o]	69.1[d]	
E_{00}	-	-	30621.6	30623[h]	30673.3	30671[h]	43646.7	43647.4[i]
B_e {rot}	0.053[b]	0.0542[k]	0.070[b]	0.0753[k]	-	-	-	-
α_e {rot}	0.00685[b]	-	0.00640[b]	0.0075[k]	-	-	-	-
D_e {rot}	2.65 $\times 10^{-6}$[b]	-	2.41 $\times 10^{-6}$[b]	-	-	-	-	-
v_D	3[a]; 4.2[c]	5[h,m]; 6[i]; 3[n]	5[a]; 6.7[d]	7[k]; 8[m]	3[a]; 3.4[c]	7[h]; 8[m]	6[a]; 7.2[d]	7[i]; 6[n]
β ($\times 10^8$ Å^{-1})	1.389	-	1.493	-	1.057	-	1.344	1.350[m]

[a] This work, BS plot. [b] This work, rotational analysis. [c] This work, LRB method. [d] This work, GvNDE program. [e] This work, Slater-Korkwood formula [36]. [f] This work, Liuti-Pirani method [17]. [g] This work, simulation of excitation spectrum. [h] Ref. [6]. [i] Ref. [8]. [j] Ref. [8], Morse approximation. [k] Ref. [7]. [l] Ref. [7], Morse approximation. [m] Ref. [9]. [n] Ref. [10]. [o] Ref. [31]. [p] Ref. [39]. [r] Refs. [37,38]. [s] Ref. [13].

same dissociation limit D'_{AB}. Concluding, the long-range tail of the $A0^+$-state potential is expressed by the formula $U'_A(R) = 30\,680.5 - 0.367 \times 10^6 R^{-6}$ cm^{-1}Å^6.

3.3.3 D1($^1\Pi$) state

Morse characteristics (see Fig. 4c and Tab. 2) for the $D1$ state were determined in a similar way than for the $B1$ and $A0^+$ states. A relationship corresponding to equation (1) written for the $D1$ state (see Fig. 1) yields the $D1$-state dissociation limit. The value obtained is 43 715.2 cm^{-1}. To obtain long-range characteristics ($n = 6$, the $^1P_1 + {}^1S_0$ atomic asymptote, see Refs. [22,24]) the GvNDE program was used and the procedure was performed similarly as for the $A0^+$ state (with a value of $C_6(D1)$, approximated in the "traditional" LRB method, v'_D from the BS analysis, and measured $E_{v'=0-2}$ as input parameters). The $C_6(D1) = 0.333 \times 10^6$ cm^{-1}Å^6, $v'_D = 7.2$ as well as D'_0 and D'_e and $E_{v'}$ up to the dissociation limit (see Fig. 4c) were obtained, and a long-range tail of the $D1$-state potential is expressed by the formula $U'_D(R) = 43\,715.2 - 0.333 \times 10^6 R^{-6}$ cm^{-1}Å^{-6}. All results for the $A0^+$, $B1$ and $D1$ excited states are collected in Table 2 and compared with those reported in other works.

3.4 $X0^+(^1\Sigma^+)$ ground state

As mentioned above, this investigation presents a *direct* determination of the CdNe ground-state characteristics. The "hot" bands were measured in both, $A0^+$, $B1 \leftarrow X0^+$ and $D1 \leftarrow X0^+$ transitions making the $X0^+$-state description more reliable and complete. Frequencies of the

Table 3. Averaged $\Delta G_{v''+1/2}$-values from vibrational "hot" bands observed in the $A0^+(^3\Pi) \leftarrow X0^+(^1\Sigma^+)$, $B1(^3\Sigma^+) \leftarrow X0^+(^1\Sigma^+)$ and $D1(^1\Pi) \leftarrow X0^+(^1\Sigma^+)$ transitions of the CdNe molecule.

v''	expt. $\Delta G_{v''+1/2}$ averaged	$\nu_1(v'-v'')-\nu_2(v'-v'')$		
		A0⁺–X0⁺	B1–X0⁺	D1–X0⁺
0	11.3	$\nu_1(0-0)-\nu_2(0-1)$ $\nu_1(1-0)-\nu_2(1-1)$ $\nu_1(2-0)-\nu_2(2-1)$	$\nu_1(0-0)-\nu_2(0-1)$ $\nu_1(1-0)-\nu_2(1-1)$ $\nu_1(2-0)-\nu_2(2-1)$	$\nu_1(0-0)-\nu_2(0-1)$ $\nu_1(1-0)-\nu_2(1-1)$
1	7.4	$\nu_1(4-1)-\nu_2(4-2)$	$\nu_1(0-1)-\nu_2(0-2)$ $\nu_1(2-1)-\nu_2(2-2)$	
2	3.5	$\nu_1(4-2)-\nu_2(4-3)$	$\nu_1(1-2)-\nu_2(1-3)$[a]	

[a] With help of the simulation (assumption of an anharmonic potential).

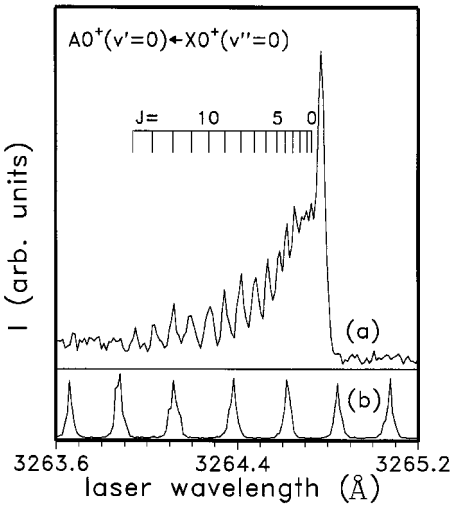

Fig. 7. (a) Rotational structure of the $v' = 0 \leftarrow v'' = 0$ band recorded in the $A0^+ \leftarrow X0^+$ transition of the excitation spectrum. (b) Fringes detected using a Fabry-Perot etalon (FSR = 1 cm^{-1}) to monitor a tuning of the fundamental laser frequency.

"hot" bands as well as corresponding $\Delta G_{v''+1/2}$ values are collected in Table 3. Using the BS plot shown in Figure 5d the $\omega_0'' = 13.2$ cm^{-1}, $\omega_0'' x_0'' = 1.94$ cm^{-1}, $D_0'' = 22.4$ cm^{-1}, and $v_{\rm D}'' = 3.4$ were obtained. It is necessary to compare these values with those of earlier investigations [6,8]. The value of ω_0'' is similar than that of Kowalski *et al.* [6], but the anharmonicity $\omega_0'' x_0''$ is approximately 30% larger and the conclusion that the previous studies [6,8–10] overestimated the D_0'' and $D_{\rm e}''$ is quite evident. Here, the dissociation energies are smaller by approximately 27–30% that those of references [6,8]. The $X0^+$-state potential well supports only four bound vibrational levels (including $v'' = 0$). The dissociation limit, D'', is related to the $v'' = 0$, therefore $D'' = D_0''$. Furthermore, using relationships (see Fig. 1):

$$D'' = D_0'' = D'_{\rm AB} - E_{\rm at}(5^3{\rm P}_1) = D'_{\rm D} - E_{\rm at}(5^1{\rm P}_1) \quad (4)$$

it is possible to relate the D'' to the dissociation limits of the considered excited states. The averaged value for D'' from equation (4) is 23.5 cm^{-1}. On the other hand, the sum $D_0'' = E_{00} + D_0' - E_{\rm at}$ gives value 23.2 cm^{-1}, as an average obtained for the three excited states. On the whole, the result for the D_0'' seems to be very consistent as determined using different approaches. In addition to that, our result allows to approximate the long-range behaviour using the potential $U''(R) = D_0'' - C_6(X0^+)R^{-6}$, as was done above for the excited states. It is justified to employ the "traditional" LRB method [22] as the measured energy of the highest $v'' = 3$ lies approximately 0.2 cm^{-1} below the dissociation limit. Figure 5b shows the LRB plot compared with that corresponding to the linear BS characteristic of Figure 4d. The $D'' = 23.4$ cm^{-1}, determined assuming a pure vdW interaction, is only slightly larger (about 1.0 cm^{-1}) than that from the BS plot.

Moreover, using the LRB method the $H_6(X0^+) = 0.66$ cm$^{-1/3}$, hence $C_6(X0^+) = 0.153 \times 10^6$ cm^{-1}Å^6, and $v_{\rm D}'' = 4.2$ were obtained (Fig. 7). The value of $v_{\rm D}''$ (LRB) is very close to that from the BS procedure corroborating the result obtained for dissociation limit: $D'' = D_0''$. Therefore, the long-range tail of the ground-state potential is expressed as $U''(R) = 23.4 - 0.153 \times 10^6 R^{-6}$ cm^{-1}Å^6. The $C_6(X0^+)$ obtained here is in perfect coincidence with that of Brym: $C_6(5^1{\rm S}_0) = 0.1566 \times 10^6$ cm^{-1}Å^6 [31]. There is always a question where is a justified limit, beyond which the long-range approximation starts. According to LeRoy [30] the approximation is valid for $R > R_{\rm LR} = 2[(\langle r^2_{\rm Cd}\rangle)^{1/2} + (\langle r^2_{\rm Ne}\rangle)^{1/2}]$, where $R_{\rm LR}$ is co-called LeRoy radius, and $\langle r_a^2\rangle$ is the expectation value of the square of the electronic radius of the unfilled valence shell of atom a. Relativistic Hartree-Fock-Slater calculations of the $\langle r_a^2\rangle$ have been reported [35], and in the case of the CdNe ground state $R_{\rm LR} = 6.38$ Å. Having determined the $C_6(X0^+)$ and employing a Slater-Kirkwood formula [36] it is possible to calculate the polarizability $\alpha_{\rm Cd}(5^1{\rm S}_0)$ of the Cd atom in the $5^1{\rm S}_0$ ground state (see also Ref. [4]). Consequently, $\alpha_{\rm Cd}(5^1{\rm S}_0) = 41.0$ a.u. (6.1 Å^3) was obtained. The result should be compared with 40.3 (±50%) a.u. ($6.0 \pm 50\%$ Å^3) [37,38], and 49.7 ± 1.6 a.u. (7.3 ± 0.2 Å^3) [39]. To obtain approximate value of the equilibrium internuclear separation in the ground state, $R_{\rm e}''$, we used a Liuti and Pirani [17] method, which employs regularities related to the vdW interactions.

The method was used recently to calculate the $R_{\rm e}''$ in CdHe [4] and ZnNe [5] complexes. In this work we obtained $R_{\rm e}''({\rm CdNe}) = 4.31$ Å. The value should be compared with $R_{\rm e}'' = 4.26$ Å of reference [7], and $R_{\rm e}'' = 4.32$ Å (see Tab. 2) obtained in this work from a rotational structure which we discuss in the next sub-section.

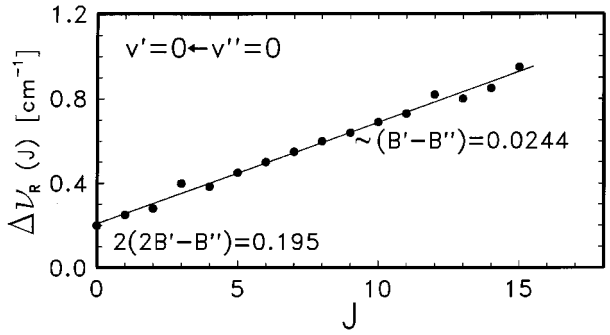

Fig. 8. Spacing between R-branch lines plotted against J in CdNe $A0^+_{v'=0} \leftarrow X0^+_{v''=0}$ transition in the excitation spectrum. The slope and the intercept with vertical axis give information on the B' and B'' rotational constants of the excited and ground states, respectively.

3.5 Rotationally resolved $A0^+_{v'=0} \leftarrow X0^+_{v''=0}$ band

Figure 7 shows the rotational structure of the $v' = 0 \leftarrow v'' = 0$ band recorded in the $A0^+ \leftarrow X0^+$ transition. The spectral bandwidth of the laser permitted to resolve particular transitions between the rotational J levels in the excites and ground states. In order to analyse the spectrum we followed the way of the earlier work of Kvaran *et al.* [7] who noticed (and so it seems) that the R-branch dominates the structure, while the P-branch lines form the band-head. We have used, to our advantage, a high purity gas (Ne) with no significant contamination by some other gases as it was the case in reference [7]. Therefore, following the arguments of Kvaran *et al.* we were able to estimate the rotational constants of the $A0^+$ and $X0^+$ states. The $\Delta\nu_J$ spacing between the R-branch lines can be expressed by the following relationship [21]:

$$\Delta\nu_J = \nu_{J+1} - \nu_J = 2(B'_{v'} - B''_{v''=0})J + 2(2B'_{v'} - B''_{v''=0}), \quad (5)$$

where $B'_{v'}$ and $B''_{v''=0}$ are inertial rotational constants in the v' and $v'' = 0$ vibrational states, respectively. Plotting $\Delta\nu_J$ *vs.* J we expect to obtain a straight-line dependence with the slope and intercept with the vertical axis equal to the $2(B' - B'')$ and $2(2B' - B'')$ values, respectively. Figure 8 presents the plot of experimental values, which lead to the evaluation of the B'_v, B''_v, B'_e, B''_e, and, eventually, to the absolute values of the equilibrium internuclear separations R_e for the ground and excited states. The rotational characteristics determined in this investigation are collected in Table 2 and compared with those reported in other studies. It is worthwhile to notice the value of $\Delta R_e = R'_e - R''_e = -0.56 \pm 0.01$ Å as it comes from our rotational analysis.

The computer simulation of the $A0^+ \leftarrow X0^+$ transition, presented in Section 3.1, yielded $\Delta R_e = -0.53 \pm 0.01$ Å, which indicates an adequate agreement of these two results and speaks favourably about the reliability of our experimental data. Consequently, the average value of the equilibrium internuclear separation $(\Delta R_e)_{aver} = -0.54 \pm 0.02$ Å, and therefore for the $A0^+$ excited and the $X0^+$ ground states we obtained $R'_e = 3.76 \pm 0.02$ Å and $R''_e = 4.32 \pm 0.02$ Å, respectively. More detailed comments and discussion on the subject of the internuclear separation will follow.

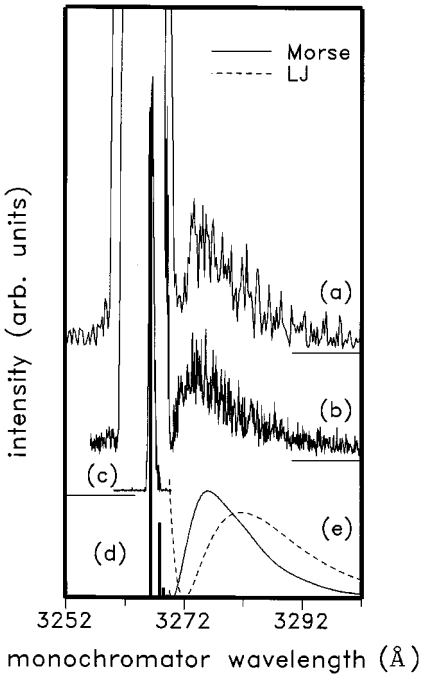

Fig. 9. (a–c) Experimental and (d–e) simulated $A0^+_{v'=1} \rightarrow X0^+$ bound-bound and bound-free parts of the fluorescence spectrum of CdNe molecule. The experimental traces were measured with $d = 150$ μm, at $X = 8$ mm distance from the orifice ($X/d = 53$), with $T_{oven} = 880$ K, $P_0 = 8.4$ atm, and (a) 200 cm^{-1}, (b) 150 cm^{-1}, and (c) 15 cm^{-1} slit-width. The simulated bound-bound and bound-free spectra were generated on the assumption of (d) Morse potential, and (e) Morse potential (solid line) and Lennard-Jones ($12.3-6$) potential (broken line) as a representation for the ground-state PE curve, with parameters derived in this study. Morse potential was assumed to represent the $A0^+$-state potential bound well.

3.6 $A0^+_{v'=1} \rightarrow X0^+$ and $D1_{v'=1} \rightarrow X0^+$ fluorescence spectra

3.6.1 Bound-bound transitions

Figure 9 presents a first-time-observed $A0^+_{v'=1} \rightarrow X0^+$ fluorescence spectrum of bound-bound and bound-free transitions of CdNe molecule. A $D1_{v'=1} \rightarrow X0^+$ spectrum, which was reported previously [8], was measured here as well. The $A0^+ \rightarrow X0^+$ and $D1 \rightarrow X0^+$ transitions arise from the decay of selectively excited $v' = 1$ vibronic levels in the $A0^+$ and $D1$ states, respectively. In both cases the transitions, which terminate on the repulsive as well as on the bound part of the ground-state PE curve, give rise to so-called Condon Internal Diffraction (CID) pattern [40]. Here, a term "reflection spectra" should be used [19] as the regular oscillations in the resulting spectrum are reflections of the squared wave function in the initial level v'.

The CID patterns continue into the bound-bound part of the spectra in the form of the FC envelope of the discrete transitions. The $A0^+ \rightarrow X0^+$ as well as not presented here $D1 \rightarrow X0^+$ profiles were recorded at different resolutions (see Figs. 9a–9c), firstly, trying to resolve the bound-bound and bound-free vibrational components, and to encompass the gross structure of the CID bands. The number of maxima in the fluorescence spectra is equal to $v'+1=2$, that confirms the v'-assignment in the spectra from Figures 2 and 3. Because of the limited resolution of the detection system, in the $A0^+_{v'=1} \rightarrow X0^+$ and $D1_{v'=1} \rightarrow X0^+$ bound-bound spectra no $v'=1 \rightarrow v''$ discrete transitions were resolved. The unresolved $v' \rightarrow v''$ components are smoothly transformed into the continuous spectra, forming the reflection structure. The computer simulation of the bound-bound part of the $A0^+ \rightarrow X0^+$ and $D1 \rightarrow X0^+$ spectra was performed assuming the Morse potential for the $A0^+$, $D1$ and $X0^+$ states, and molecular parameters derived in the analysis of the excitation spectrum (see Sect. 3.3).

A result of the simulation of a short-wavelength part of the $A0^+_{v'=1} \rightarrow X0^+_{v''}$ spectrum, *i.e.*, the bound-bound transitions, is shown in Figure 9d. The "best fit" of the computer simulation is juxtaposed with the experimental profiles, which in case of bound-bound transitions in the $A0^+ \rightarrow X0^+$ (as well as in $D1 \rightarrow X0^+$) fluorescence constitute the most short-wavelength peak of the corresponding spectrum. In the next step of the analysis we considered the bound-free transitions that reflect a fluorescence terminating on the repulsive part of the ground-state potential, *above* its dissociation limit. Here, the determination of the $X0^+$ potential wall is very accurate as we used two *independent* fluorescence channels.

3.6.2 Bound-free transitions: determination of the X0$^+$-state potential above its dissociation limit

Figures 9a and 9b shows a gross structure of the $A0^+_{v'=1} \rightarrow X0^+$ transition. It (as well as $D1_{v'=1} \rightarrow X0^+$) was detected for $d=150$ μm, at $X=8-9$ mm, with $T_{\mathrm{oven}}=800-880$ K and $p_0=8.4-9.2$ atm. The measured trace spreads out over the wide range of wavelengths from 3252 Å to 3302 Å (from 2278 Å to 2312 Å in case of the $D1 \rightarrow X0^+$). Having identified the particular vibrational level of the $A0^+$ or $D1$ state, which was populated with a specific laser wavelength, and from which the fluorescence was emitted, the next step was to proceed with the determination of the $X0^+$ repulsive wall *above* the dissociation limit.

The procedure was to assume the repulsive potential of a certain form with a free parameter (or parameters), and then to simulate the bound-free spectrum using this potential, and vary the parameter(s) (using a trial and error approach) to obtain the best agreement between the observed and calculated positions of the maximum. The simulations were made separately for the $A0^+$ and $D1$ states assuming the same "trial" potential for the ground state. The $A0^+$ and $D1$ excited states were represented by Morse functions with parameters determined in this study. Initially, a *Morse* function was assumed as representative of the $X0^+$ state potential [21]:

$$U''_{\mathrm{Mor}}(R) = D''_{\mathrm{e}}[1-\exp(-\beta(R-R''_{\mathrm{e}}))]^2, \qquad (6)$$

where $\beta = (8\pi^2 c\mu\omega''_{\mathrm{e}}x''_{\mathrm{e}}/h)^{1/2}$, $\omega''_{\mathrm{e}} \approx \omega''_0 + \omega''_0 x''_0$ (see Tab. 2). The computer-simulation program and the procedure is described in detail elsewhere [42]. We used a BCONT 1.4 FORTRAN code of LeRoy [43] and assumed that the electronic dipole transition moment M does not change with R. The calculations were performed for a rotationless structure in the upper and lower states [44]. In the experiments with molecules produced in the supersonic expansion beam the lowest J'' and J' levels, belonging to particular vibronic v'' and v' levels, respectively, are populated, and a collisional mixing between rotational levels is negligible [45]. The simulated $A0^+_{v'=1} \rightarrow X0^+$ bound-free spectrum is presented in Figure 9e. The solid line represents the situation when the ground-state potential is described by a Morse function. It is evident from the simulated profile that with the $X0^+$-state spectroscopic constants derived in the analysis of the excitation spectrum the ground state potential above the dissociation limit can be represented by the Morse function as well. The same conclusion was attained in the simulation of the $D1_{v'=1} \rightarrow X0^+$ spectrum.

During the simulation procedure we also applied other functions to represent the CdNe ground-state potential. As in the case of the HgAr [46,47] and HgKr [48] molecules the $X0^+$ repulsive wall was represented by the *Lennard-Jones* (n-6) (LJ) potential (*e.g.* [49]), which was also successfully used earlier to represent a mercury dimer ground-state potential [42]:

$$U''_{\mathrm{LJ}}(R) = \frac{D''_{\mathrm{e}}}{n-6}[6(R''_{\mathrm{e}}/R)^n - n(R''_{\mathrm{e}}/R)^6], \qquad (7)$$

where n is the parameter estimated from the relation

$$\mathrm{d}^2U''(R=R''_{\mathrm{e}})/\mathrm{d}R^2 = 2\pi c\omega''_{\mathrm{e}} \qquad (8)$$

within the harmonic oscillator approximation (*e.g.* [46,49,50]). Equation (8) should be satisfied by every analytically reasonable potential. For the LJ (n-6) representation, equation (8) gives an expression for the parameter n:

$$n = 2\pi^2\mu c(\omega''_{\mathrm{e}})^2(R''_{\mathrm{e}})^2/3hD''_{\mathrm{e}}. \qquad (9)$$

By substituting into equation (9) values for $\mu = 17.108 \times 1.66\times10^{-24}$ g for CdNe, and ω''_{e}, D''_{e} and R''_{e} from the analysis of the excitation spectrum, $n=12.3$ was calculated. The result of the simulation is shown in Figure 9e (broken line). A comparison with the experimental $A0^+_{v'=1} \rightarrow X0^+$ trace as well as with the profile simulated earlier (Morse function, solid line) leads to the conclusion that the LJ (n-6) potential (7), is not a good representation of the $X0^+$ state repulsive wall. The simulated profile spreads out far into the long-wavelength region, indicating that the LJ (12.3-6) potential is too steep. Similar conclusion was attained while simulating the $D1_{v'=1} \rightarrow X0^+$ spectrum.

Another alternative for the CdNe ground-state representation is provided by a *Maitland-Smith* (n_0, n_1) (MS) potential [51], which is the LJ (n-6) potential (7) with the parameter $n = n_0 + n_1(R/R''_e - 1)$. The MS($n_0$, n_1) potential was applied previously for metal-rare gas complexes by Koperski [46,47] as well as Koperski *et al.* [48], and Findeisen and Grycuk [52] to represent the interatomic potential of the HgAr and HgKr ground states. Preliminary results show that the ground state of other CdRG and ZnRG molecules can be represented by the MS potential as well [53]. The MS(n_0, n_1) potential should satisfy equation (8), which produces an expression for n_0 similarly as equation (9) does for n. The advantage is evident: $n_0 = 12.3$ can be fixed as a result of the condition in equation (8) and there is still one free parameter n_1, which may be found from the "best fit" to the experimental spectrum. However, to obtain the explicit expression for the MS(n_0, n_1) potential as properly describing its repulsive part, n_0 has to be larger than n_1 as $U(R \to 0) \to \infty$. This produces a *unique pair* of the parameters (n_0, n_1) that defines the unique MS(n_0, n_1) potential, which fits to the experimental spectrum.

From a detailed comparison of the simulated and observed $A0^+_{v'=1} \to X0^+$ and $D1_{v'=1} \to X0^+$ profiles it was not possible to find a MS(n_0, n_1) function that would satisfy the above requirements. The "best fit" for the $X0^+$-state repulsive wall was found to be of the form of the MS representation with $n_1 > n_0 = 12.3$. This produces a singularity ($U(R) \to -\infty$) as $R \to 0$ and can not be accepted as a good representation for the molecular PE curve.

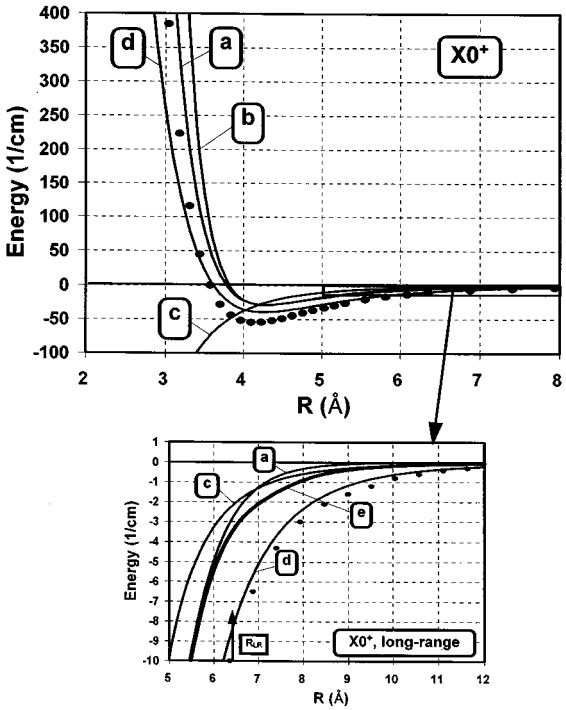

Fig. 10. PE curves for the $X0^+(^1\Sigma^+)$ electronic energy state of CdNe molecule. Potentials derived in this investigation and represented by (a) Morse, (b) L-J (n-6), $n = 12.3$, and (c) $-C_6(X0^+)R^{-6}$, $C_6(X0^+) = 0.153 \times 10^6$ cm^{-1}Å^6, functions. Earlier experimental representation of (d) Funk *et al.* [8], and *ab initio* points of Czuchaj and Stoll [13] (•) are shown. Insert presents a detailed view from the rectangle in the long-range limit, close to the dissociation. (a), (c), (d) and (•) as above; (e) combined Morse-vdW potential (see text). The LeRoy radius R_{LR} is depicted.

4 Discussion – PE curves for the ground and excited states

4.1 CdNe ground-state potential

Based on the experimental evidence, we found that the analytical function, which describes the CdNe ground-state potential differs from those obtained in previous investigations of the complex. Figure 10 shows PE curves of the ground state derived in this investigation compared with those plotted according to the experimental result of Funk *et al.* [8] as well as theoretical data of Czuchaj and Stoll [13]. The potential of reference [8] has larger dissociation energy. The theoretical result of Czuchaj and Stoll [13] obtained using *ab initio* atomic core-valence atoms interaction calculation shows even deeper potential with a shorter bond length than the experimental ones. The bound-free fluorescence emitted from $v' = 1$ vibronic levels of the $A0^+$ and $D1$ states was observed out to about 3302 Å and 2311 Å, respectively. Therefore, the ground-state repulsive branch can be mapped accurately up to a point approximately 360−390 cm^{-1} above the dissociation energy [54]. This corresponds to a 3.15−3.75 Å region of internuclear separations within which the present characterisation *above* the dissociation limit was performed. Besides the Morse (curve (a)) and the L-J (12.3-6) potential (curve (b)) Figure 10 presents also a $-C_6(X0^+)R^{-6}$-type long-range approximation, where $C_6(X0^+)$ was obtained using the "traditional" LRB method. The region *below* the dissociation limit consists of two parts: in the vicinity of the potential well (from 3.75 Å to the R_{LR}) and the part of the long-range tail ($R > R_{LR}$). According to the above analysis the former is represented by the Morse function, which represents also the repulsive part of the potential. The long-range of the internuclear separations from Figure 10 is shown in detail in an insert of Figure 10.

To represent accurately the long-range tail of the potential it is possible to use an approach of a hybrid potential (*e.g.* [46,47]) or to follow a suggestion of Zimmermann and co-workers (*e.g.* [55]) and applied so-called a combined Morse-vdW potential:

$$U''_{M-vdW}(R) = D''_e[1 - \exp(-\beta(R - R''_e))]^2 - D''_e - [1 - \exp(-(R - R_c)^{12})]C_6(X0^+)R^{-6}. \quad (10)$$

The potential (10) was successfully employed elsewhere to represent PE curves of ground and excited states of NaRG complexes [55]. In equation (10) the expression $[1 - \exp(-(R - R_c)^{12})]$ was used to allow for smooth junction of the two, Morse and $-C_6(X0^+)R^{-6}$ potentials,

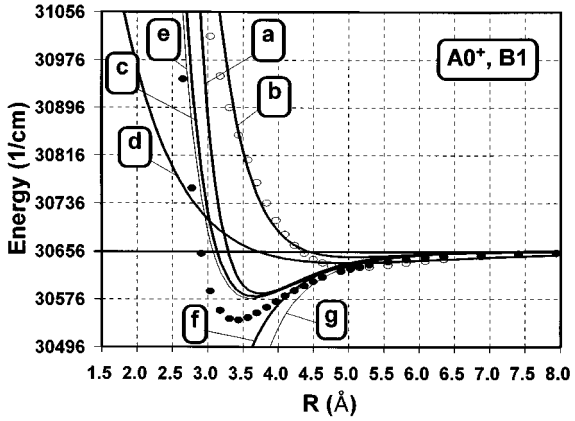

Fig. 11. PE curves for the $A0^+(^3\Pi)$ and $B1(^3\Sigma^+)$ electronic energy states of CdNe molecule. (a) and (b) $A0^+$ and $B1$-state Morse potentials, respectively, derived in this investigation; (c) and (d) $A0^+$ and $B1$-state Morse potentials, respectively, obtained previously by Bobkowski *et al.* [9]; (e) $A0^+$-state Morse potential of Kvaran *et al.* [7]; (f) $-C_6(B1)R^{-6}$, $C_6(B1) = 0.37 \times 10^6$ cm^{-1}Å^6, representation of this study; (g) $-C_6R^{-6} + C_{12}R^{-12}$, $C_6 = 3.991 \times 10^5$ cm^{-1}Å^6 and $C_{12} = 5.38 \times 10^8$ cm^{-1}Å^{12} representation of reference [7]; (•) and (○) theoretical *ab initio* points of Czuchaj and Stoll [13] for the $A0^+$ and $B1$ potential, respectively.

and R_c denotes a distance where the Morse joins the long-range vdW potential. Here, we set $R_c = 7$ Å as the value for which the Morse potential crosses the $-C_6(X0^+)R^{-6}$ tail (note that $R_c > R_{LR}$). The function (10) can be used as a representation of the CdNe ground-state potential not only in the long-range region but also for $R < R_{LR}$ as it overlaps the Morse potential for smaller R [56]. For the sake of comparison the insert in Figure 10 shows also the potential of reference [8] and the theoretical points of Czuchaj and Stoll [13]. Summarising, we postulate a new potential for the ground state of CdNe molecule, determined from the experimental data presented in this study:

$$U''_{M-vdW}(R) = 28.3[1 - \exp(-1.389(R - 4.28))]^2 - 28.3 - [1 - \exp(-(R - 7.0)^{12})]0.153 \times 10^6 R^{-6}, \quad (11)$$

where U'' and R are expressed in cm^{-1} and Å, respectively.

4.2 A0$^+$($^3\Pi$), B1($^3\Sigma^+$) and D1($^1\Pi$) excited states potentials

Figure 11 shows PE curves for the CdNe excited states which correlate to the 5^3P_1 Cd atomic asymptote. The $A0^+(^3\Pi)$ and $B1(^3\Sigma^+)$-states interatomic potentials derived in this investigation are compared with those of Kvaran *et al.* [7] and Bobkowski *et al.* [9] as well as with theoretical result of Czuchaj and Stoll [13]. The reinterpretation of the $B1 \leftarrow X0^+$ excitation spectrum lead to a new $B1$-state interatomic potential, which has a larger bond length and shorter bond strength than the experimental and theoretical potentials of references [9,13], respectively. The $A0^+$-state potential differs from those of other studies [7,9,13] as well. The one determined here is shallower and has a larger bond length than the experimental potentials of Kvaran *et al.* [7] and Bobkowski *et al.* [9], and theoretical result of Czuchaj and Stoll [13]. The long-range characteristics of the $A0^+$ and $B1$ states are compared in Table 2 with the experimental $C_6(A0^+)$ constant of reference [7] and theoretical result of Brym [31], respectively. A graphical comparison of the PE curves (not presented here) shows that the long-range tails decrease to the value of the dissociation limit at a slower rate than the Morse representation confirming the non-Morse behaviour of the $A0^+$ and $B1$ potentials in the long-range limit.

The parameters of the $D1(^1\Pi)$-state potential derived here are compared in Table 2 with those of Funk *et al.* [8] and Czajkowski *et al.* [10] as well as with theoretical result of reference [13]. Except of the result of Czuchaj and Stoll [13] all experimental potentials are very similar and differ only slightly from each other. Hence, one tends to believe that the $D1$-state potential derived from *ab initio* calculation yields potential well too deep with too short bond length. The first-time obtained long-range tail of the $D1$-state potential compared graphically with the Morse representations of references [8,10] (not presented here) confirms than the potentials of earlier investigations decrease to the value of dissociation energy quicker than the long-range tail of this study, *i.e.* that the $D1$-state potential has a non-Morse component for large internuclear separations as well.

4.3 Comparison with CdRG and MeNe molecules

Tables 4 and 5 present a comparison of spectroscopic characteristics of the $X0^+(^1\Sigma^+)$ and $B1(^3\Sigma^+)$ states for CdRG and the ground states of MeNe molecules, respectively. As expected, within the CdRG family (Tab. 4), for the dissociation energies of the $X0^+$ and $B1$ states, the tendency is distinct and fairly consistent. The D''_e and D'_e *increase* as a mass of the RG atom *increases*. The similar trend is observed within the MeNe family (Tab. 5). As a mass of the metal atom *increases* the D''_e *increases* as well. The opposite is observed for the bond lengths R''_e. They *decrease* as the mass of the RG or Me atom increases. In the CdRG family, the long-range coefficient C''_6 which is, according to reference [29] expressed by the Slater-Kirkwood formula [36], *increases* as the mass of the RG atom increases. It illustrates a general tendency, which describes the long-range tail of the ground-state potential assuming that only the vdW force is in effect and fully describes the interaction between the Cd and RG atoms in this region of internuclear separations.

At this point it is necessary to comment on several characteristics determined earlier [4,12], and which were re-evaluated during the course of this work. The value for the equilibrium internuclear separation of the CdHe ground state was mistakenly reported as to be $R''_e = 4.42$ Å (see Tab. 2 of Ref. [4]) while the correct

Table 4. Comparison of the $X0^+(^1\Sigma^+)$ and $B1(^3\Sigma^+)$-state characteristics for the CdRG molecules.

Molecule	$X0^+(^1\Sigma^+)$			$B1(^3\Sigma^+)$	
	D_e'' [cm^{-1}]	R_e'' [Å]	C_6'' [a.u.] [j]	D_e' [cm^{-1}]	R_e' [Å]
CdHe [a]	14.2	4.33	17.7	6.1	4.45
CdNe	28.3 [b]	4.26 [c] 4.32 [h]	35.5 31.7 [h]	9.6 [b]	5.12 [b]
CdAr	106 [d] 106.5 [e]	4.31 [d] 4.33 [f] 4.28 [h]	134.2	59.7 [c]	5.03 [c]
CdKr	129 [d] 114.4 [g] 173.6 [i]	4.5 [g] 4.2 [h] 4.12 [i]	193.0 164.3 [i]	60.2 [g]	5.07 [g]
CdXe	274.6 [i]	4.18 [h]	298.0	226.3 [i]	4.23 [i]

[a] Ref. [4], see comment in text (Sect. 4.3). [b] This work. [c] Ref. [7]. [d] Ref. [8]. [e] Ref. [9]. [f] Ref. [7]. [g] Ref. [57]. [h] Liuti and Pirani method [17], see text. [i] Ref. [53]. [j] Slater-Kirkwood formula [36].

value should read $R_e''(\mathrm{CdHe}) = 4.33$ Å. The result has an influence on the values of the $R_e'(A0^+)$ and $R_e'(B1)$ in CdHe as they were deduced from precisely determined differences $\Delta R_e = R_e'' - R_e'$. Therefore, the corrected equilibrium internuclear separations for the CdHe excited states are $R_e'(A0^+) = 2.83$ Å and $R_e'(B1) = 4.45$ Å (see Tab. 4). In the spectroscopic studies of the HgNe complex of Koperski *et al.* [12] the observed first energetic separation in the ground state was interpreted as ω_0'', while in the anharmonic potential approximation this value corresponds to $\omega_0'' - \omega_0'' x_0''$. This changes slightly spectroscopic characteristics of the HgNe ground state that were derived in reference [12]. The correct values that should replace those from Table 2 of reference [12] are as follows: $\omega_0'' = 18.0$ cm^{-1}, $\omega_0'' x_0'' \approx \omega_e'' x_e'' = 2.56$ cm^{-1}, $\omega_e'' = 20.6$ cm^{-1}, $D_0'' = 31.7$ cm^{-1} and $D_e'' = 41.4$ cm^{-1} (see Tab. 5).

5 Conclusions

Since the first characterisation of the ground and lowest excited states of the CdNe complex in 1985 [6], there have been four other studies [7–10] that dealt with the spectroscopy of this vdW molecule. Indirect characterisation of the ground state, dubious interpretation of the $B1 \leftarrow X0^+$ transition in the excitation spectrum and questionable characterisation of the $B1(^3\Sigma^+)$ excited state called for additional investigation.

In this work we presented a first-time observed $A0^+_{v'=1} \rightarrow X0^+$ fluorescence spectrum as well as a repeated measurement of the $D1_{v'=1} \rightarrow X0^+$ fluorescence, and $A0^+_{v'} \leftarrow X0^+_{v''=0,1,2}$, $B1_{v'} \leftarrow X0^+_{v''=0,1,2}$ and $D1_{v'} \leftarrow X0^+_{v''=0,1}$ transitions in the excitation spectrum of the CdNe vdW complex. The experiment was performed in a supersonic molecular continuous free-jet combined with the excitation by means of a UV pulsed-laser beam. Selecting a suitable region of the expansion we efficiently detected "hot" bands in the excitation spectrum that provided a direct information on the D_0''. A good signal-to-noise ratio in the detection of $B1 \leftarrow X0^+$ transition in the excitation spectrum allowed us to accurately determine a number of bound v' levels in the $B1$-state potential well.

Table 5. Comparison of the ground-state characteristics for the MeNe molecules.

Molecule	m_{Me} [amu]	D_e'' [cm^{-1}]	R_e'' [Å]	ω_e'' [cm^{-1}]	$\omega_e'' x_e''$ [cm^{-1}]
ZnNe [a]	65.4	20.2	4.40	14.8	2.7
CdNe	112.4	28.3 [b]	4.32 [b]	15.0 [b]	1.94 [b]
HgNe	200.6	41.4 [c] 46 [d]	3.89 [c] 3.90 [d]	20.6 [c] 18.5 [d]	2.56 [c] 1.6 [d]

[a] Ref. [5]. [b] This work. [c] Ref. [12], see comment in text (Sect. 4.3). [d] Ref. [11].

Moreover, we detected separately two "channels" of fluorescence started from selectively excited vibrational levels in different electronic energy states and terminated on the same repulsive part of the ground-state PE curve. The recorded spectra were subjected to an improved analysis based on a complete simulation of bound-free and bound-bound parts. The analysis allowed to determine accurately spectroscopic constants for all four states involved in the investigation. Particularly, the characterisation was improved for the $B1$ and $X0^+$ states. Moreover, in the simulation of the $A0^+ \leftarrow X0^+$ progression in the excitation spectrum we allowed for an influence of the intense atomic line on the FC-intensity distribution. This changed previously known value for the ΔR_e in the $A0^+$ and ground states. The analysis of the rotationally resolved $v' = 0 \leftarrow v'' = 0$ band in the $A0^+ \leftarrow X0^+$ transition of the excitation spectrum allowed to determine several rotational characteristics for the $A0^+$ and ground states, and the absolute value for the $X0^+$-state equilibrium internuclear separation. The obtained results indicate that a Morse function combined with an adequate long-range approximation represent the interatomic potential energy curve of the $A0^+$, $B1$, $D1$ and $X0^+$ states *below* the dissociation limit. The repulsive part of the ground state *above* the dissociation limit was accurately modelled in the range from 3.15 Å to 3.75 Å, and was represented by the Morse potential.

The importance of such an investigation for the field of laser cooling and optical trapping [1] as well as the matter-wave interferometry [2] has been stressed.

This research was supported by a grant from the Natural Science and Engineering Research Council of Canada. One of us (J.K.) was supported also by the Polish State Committee for Scientific Research (K.B.N.) grant # 2 P03B 107 10.

References

1. P.D. Lett, P.S. Julienne, W.D. Phillips, Ann. Rev. Phys. Chem. **46**, 423 (1995).
2. C. Champenois, E. Audouard, P. Duplàa, J. Vigué, J. Phys. II France **7**, 523 (1997); R.C. Forrey, L. You, V. Kharchenko, A. Dalgarno, Phys. Rev. A **55**, R3311 (1997).
3. W.H. Breckenridge, C. Jouvet, B. Soep, in *Advances in Metal and Semiconductor Clusters*, edited by M. Duncan (JAI Press Inc., 1995), Vol. 3, p. 1.
4. J. Koperski, M. Czajkowski, J. Chem. Phys. **109**, 459 (1998).
5. J. Koperski, M. Czajkowski, Phys. Rev. A (accepted).
6. A. Kowalski, M. Czajkowski, W.H. Breckenridge, Chem. Phys. Lett. **121**, 127 (1985).
7. A. Kvaran, D.J. Funk, A. Kowalski, W.H. Breckenridge, J. Chem. Phys. **89**, 6069 (1988).
8. D.J. Funk, A. Kvaran, W.H. Breckenridge, J. Chem. Phys. **90**, 2915 (1989).
9. R. Bobkowski, M. Czajkowski, L. Krause, Phys. Rev. A **41**, 243 (1990).
10. M. Czajkowski, L. Krause, R. Bobkowski, Phys. Rev. A **49**, 775 (1994).
11. K. Yamanouchi, S. Isogai, N. Okunischi, S. Tsuchiya, J. Chem. Phys. **88**, 205 (1988).
12. J. Koperski, J.B. Atkinson, L. Krause, Chem. Phys. **186**, 401 (1994).
13. E. Czuchaj, H. Stoll, Chem. Phys. **248**, 1 (1999).
14. A. Nesmeyanov, *Vapor pressure of the elements* (Academic Press, New York, 1963).
15. L.B. Lubman, C.T. Rettner, R.N. Zare, J. Phys. Chem. **86**, 1129 (1982).
16. R. Campargue, J. Phys. Chem. **88**, 4466 (1984).
17. G. Liuti, F. Pirani, Chem. Phys. Lett. **122**, 1245 (1985); R. Cambi, D. Cappelletti, G. Liuti, F. Pirani, J. Chem. Phys. **95**, 1852 (1991).
18. E.U. Condon, Phys. Rev. **32**, 858 (1928).
19. J. Tellinghuisen, Phys. Rev. Lett. **34**, 1137 (1975); in *Photodissociation and Photoionization*, edited by K.P. Lawley (J. Wiley and Sons, 1985), p. 299.
20. R.T. Birge, H. Sponer, Phys. Rev. **28**, 259 (1926).
21. G. Herzberg, *Molecular Structure and Molecular Spectra. I. Spectra of Diatomic Molecules*, 2nd edn. (D. van Nostrand, 1950).
22. R.J. Le Roy, R.B. Bernstein, J. Chem. Phys. **52**, 3869 (1970); Chem. Phys. Lett. **5**, 42 (1970); J. Mol. Spectrosc. **37**, 109 (1971).
23. W.C. Stwalley, Chem. Phys. Lett. **6**, 241 (1970); J. Chem. Phys. **58**, 3867 (1973).
24. R.J. LeRoy, J. Chem. Phys. **101**, 10217 (1994); J. Chem. Phys. **73**, 6003 (1980).
25. R.J. Le Roy, J. Chem. Phys. **73**, 6003 (1980); R.J. Le Roy, W.-H. Lam, Chem. Phys. Lett. **71**, 544 (1980).
26. J.W. Tromp, R.J. Le Roy, J. Mol. Spectrosc. **109**, 352 (1985); K.J. Jordan, R.H. Lipson, N.A. McDonald, R.J. Le Roy, J. Phys. Chem. **96**, 4778 (1992).
27. A. Fioretti, D. Comparat, C. Drag, C. Amiot, O. Dulieu, F. Masnou-Seeuws, P. Pillet, Eur. Phys. J. D **5**, 389 (1999).
28. J. Koperski, J. Chem. Phys. **105**, 4920 (1996).
29. R.J. Le Roy (private communication). Substituting $(v_{\rm D} - v) = \Delta G_v^2 \omega_{\rm e} x_{\rm e}$ into the expression $E_v = D_{\rm e} - \omega_{\rm e} x_{\rm e} (v_{\rm D} - v)^2$, which is the same as the integrated form of equation (3) with $\omega_{\rm e} x_{\rm e}$ replacing $K_n(n-2)/2n$, one obtains $(E_v - D_{\rm e}) \sim \Delta G_v^2$, *i.e.* $D_{\rm e}$ is provided as an intercept of the ΔG_v^2 *vs.* E_v plot with the horizontal axis.
30. R.J. LeRoy, in *Molecular Spectroscopy*, edited by R.F. Barrow, D.A. Long, D.J. Millen (London, 1973), Vol. I: A Specialist Periodical Report of the Chemical Society, p. 113.
31. S.H. Brym, Habilitation thesis, Pedagogical University, Olsztyn, 1996, p. 101, Table 6.3 (*in Polish*).
32. C.J.K. Quayle, I.M. Bell, E. Takács, X. Chen, K. Burnett, D.M. Segal, J. Chem. Phys. **99**, 9608 (1993).
33. L. Krim, B. Soep, J.P. Visticot, J. Chem. Phys. **103**, 9589 (1995).
34. D. Segal, I.D. Harris, J. Chem. Phys. **94**, 2713 (1991).
35. C.C. Lu, T.A. Carlson, F.B. Malik, T.C. Tucker, C.W. Nestor Jr, At. Data **3**, 1 (1971).
36. J.C. Slater, J.G. Kirkwood, Phys. Rev. **37**, 682 (1931).
37. *Handbook of Chemistry and Physics*, edited by D.R. Lide, 72nd edn. (RCR Press, 1991-1992); *Science Data Book*, edited by R.M. Tennent (Oliver & Boyd, Edinburgh, 1976).
38. T.M. Miller, B. Bederson, Adv. At. Mol. Phys. **13**, 1 (1977).
39. D. Goebel, U. Hohm, Phys. Rev. A **52**, 3691 (1995).
40. E.U. Condon, Phys. Rev. **32**, 858 (1928).
41. R.S. Mulliken, J. Chem. Phys. **55**, 309 (1971).
42. J. Koperski, J.B. Atkinson, L. Krause, J. Mol. Spectrosc. **184**, 300 (1997).
43. R.J. LeRoy, Comput. Phys. Comm. **52**, 383 (1989); R.J. LeRoy, BCONT 1.4; *A Computer Program for Calculating Absorption Coefficients (Emission Intensities or Golden Rule) Predissociation Rates*, University of Waterloo, Chemical Physics Research Report CP-329R^3 (1993, unpublished).
44. D.E. Pritchard, F.Y. Chu, Phys. Rev. A **2**, 1932 (1970).
45. Thus, it is justified to assume that the levels with higher J'' and J' were not populated. When the transitions with $J \neq 0$ are included in the simulations, a slight broadening of the oscillatory maxima and a little change in intensity at the minima will occur; see also references [46].
46. J. Koperski, Chem. Phys. **211**, 191 (1996).
47. J. Koperski, Chem. Phys. **214**, 431E (1997).
48. J. Koperski, J.B. Atkinson, L. Krause, J. Mol. Spectrosc. (submitted).
49. D. Eisel, D. Zevgolis, W. Demtröder, J. Chem. Phys. **71**, 2005 (1979).
50. I. Wallace, J. Ryter, W.H. Breckenridge, J. Chem. Phys. **96**, 136 (1992).
51. G.C. Maitland, E.B. Smith, Chem. Phys. Lett. **22**, 443 (1973).
52. M. Findeisen, T. Grycuk, J. Phys. B: At. Mol. Opt. Phys. **22**, 1583 (1989).
53. J. Koperski, M. Czajkowski (unpublished).
54. This limit is obtained by subtracting the energy of 3302 Å or 2311 Å photon from the energy of the $A0^+_{v'=1}$ or $D1_{v'=1}$ levels emitting the fluorescence spectra, respectively.
55. P. Baumann, D. Zimmermann, R. Brühl, J. Mol. Spectrosc. **155**, 277 (1992).
56. Using equation (23) changes slightly the $D''_{\rm e}$ (*i.e.* increases it by 0.2%) with respect to that obtained from pure Morse approximation.
57. M. Czajkowski, R. Bobkowski, L. Krause, Phys. Rev. A **44**, 5730 (1991).